

# ALMA reveals a candidate hot and compact disk around the O-type protostar IRAS 16547–4247

Luis A. Zapata<sup>1</sup>, Aina Palau<sup>1</sup>, Roberto Galván-Madrid<sup>1,2</sup>, Luis F. Rodríguez<sup>1</sup>, Guido Garay<sup>3</sup>, James M. Moran<sup>4</sup>, and Ramiro Franco-Hernández<sup>3</sup>

<sup>1</sup>Centro de Radioastronomía y Astrofísica, Universidad Nacional Autónoma de México, 58089 Morelia, Michoacán, México

<sup>2</sup>European Southern Observatory, Karl-Schwarzschild-Str. 2, D-85748 Garching, Germany

<sup>3</sup>Departamento de Astronomía, Universidad de Chile, Casilla 36-D, Santiago, Chile

<sup>4</sup>Harvard-Smithsonian Center for Astrophysics, 60 Garden Street, Cambridge, MA 02138

Accepted 15 October 2018. Received 15 October 2018; in original form 15 October 2018

## ABSTRACT

We present high angular resolution ( $\sim 0.3''$ ) submillimeter continuum (0.85 mm) and line observations of the O-type protostar IRAS 16547–4247 carried out with the *Atacama Large Millimeter/Submillimeter Array* (ALMA). In the 0.85 mm continuum band, the observations revealed two compact sources (with a separation of  $2''$ ), one of them associated with IRAS 16547–4247, and the other one to the west. Both sources are well resolved angularly, revealing a clumpy structure. On the other hand, the line observations revealed a rich variety of molecular species related to both continuum sources. In particular, we found a large number of S-bearing molecules, such as the rare molecule methyl mercaptan ( $\text{CH}_3\text{SH}$ ). At scales larger than 10,000 AU, molecules (*e.g.*,  $\text{SO}_2$  or  $\text{OCS}$ ) mostly with low excitation temperatures in the upper states ( $E_k \lesssim 300$  K) are present in both millimeter continuum sources, and show a southeast-northwest velocity gradient of  $7 \text{ km s}^{-1}$  over  $3''$  ( $165 \text{ km s}^{-1} \text{ pc}^{-1}$ ). We suggest that this gradient probably is produced by the thermal (free-free) jet emerging from this object with a similar orientation at the base. At much smaller scales (about 1000 AU), molecules with high excitation temperatures ( $E_k \gtrsim 500$  K) are tracing a rotating structure elongated perpendicular to the orientation of the thermal jet, which we interpret as a candidate disk surrounding IRAS 16547–4247. The dynamical mass corresponding to the velocity gradient of the candidate to disk is about  $20 M_\odot$ , which is consistent with the bolometric luminosity of IRAS 16547–4247.

**Key words:** stars: pre-main sequence – ISM: jets and outflows – individual: (IRAS 16547–4247) – individual: (G343.14-0.05)

## 1 INTRODUCTION

Recent theoretical studies by Krumholz et al. (2009), Peters et al. (2010), and Kuiper et al. (2010) have demonstrated that stars up to  $140 M_\odot$  can be formed in a similar way to the low- and intermediate-mass stars, that is, through flattened accretion disks. The existence of disks around high-mass stars solves the long-standing radiation pressure problem, where the powerful radiation pressure of the star is expected to halt the infalling material. However, at this point, there is a lack of detections of centrifugally supported circumstellar disks surrounding young O-type stars due probably to the large distances of the stars (a few kpc), their very small number, and the complexity of the regions of massive star formation (*e.g.*, Zinnecker & Yorke 2007; Zapata et al. 2011; Naranjo-Romero et al. 2012).

There are a few cases where disks rotationally supported are present in young O-type stars associated with a large luminosity (of about  $10^{4-5} L_\odot$ ): AFGL2591-VLA3, Wang et al. (2012);

Jiménez-Serra et al. (2012); IRAS 18360-0537, Qiu et al. (2012); NGC 7538 IRS1, Moscadelli & Goddi (2014); Klaassen et al. (2009); Hoffman (2012); W51 North, Zapata et al. (2009, 2010); W33A, Galván-Madrid et al. (2010). In the cases of IRAS 18360-0537, NGC 7538 IRS1, and W51 North there is some evidence that the innermost parts of the disks are Keplerian, similar to the rotating structures found in low-mass stars. It is important to note that most of these structures are  $\gtrsim 5000$  AU in size (with the exception of AFGL 2591 and NGC 7538), and most likely are forming systems of massive stars.

IRAS 16547–4247 (*hereafter* IRAS 16457) is catalogued as a young massive protostar with a bolometric luminosity of  $6.2 \times 10^4 L_\odot$  (Garay et al. 2003), equivalent to that of a single O8 zero-age main-sequence star (Panagia 1973), although it is probably a cluster for which the most massive source would have a slightly lower luminosity. The source is located at a distance of  $2.9 \pm 0.6$  kpc (Rodríguez et al. 2008). Observations at radio wavelengths have revealed a triple continuum source that is aligned in a northwest-

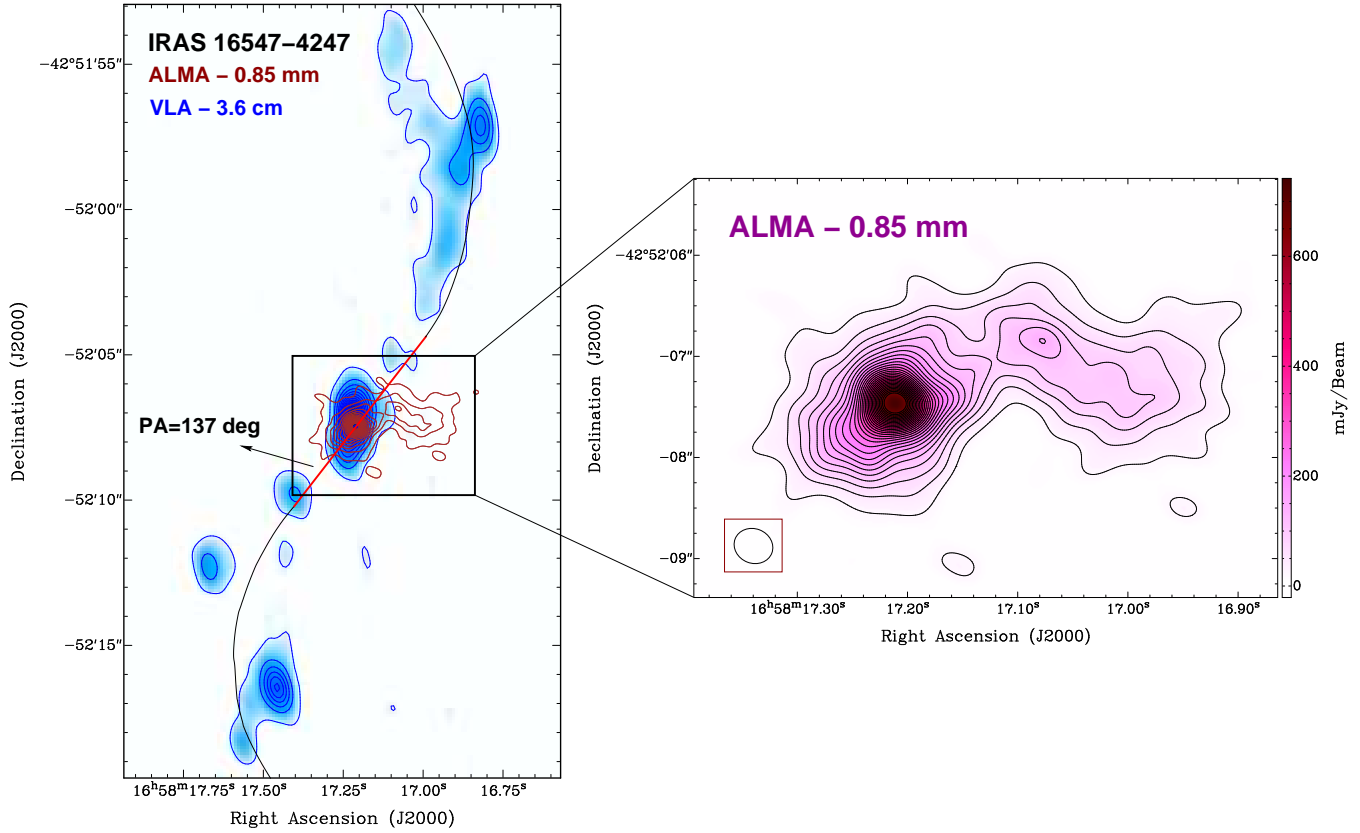


**Figure 1.** 3.6 cm and 0.85 mm continuum color-scale/contours images from IRAS 16547 obtained with the Very Large Array (Rodríguez et al. 2008) and The Atacama Large Millimeter/Submillimeter Array (this work), respectively. The blue color-scale/contours show the continuum emission arising at 3.6 cm, while the violet color-scale/contours show the continuum emission at 0.85 mm. Note that the 3.6 cm continuum emission traces a radio thermal (free-free) jet with an orientation northwest-southeast (Rodríguez et al. 2008; Garay et al. 2003), while the emission detected by ALMA is only present in the middle and traces dust thermal emission. The blue contours range from 5% to 90% of the peak emission, in steps of 5%. The peak of the centimeter continuum emission is  $6 \text{ mJy beam}^{-1}$ . The brown contours range from 5% to 90% of the peak emission, in steps of 5%. The violet contours (on the right panel) range from 6% to 90% of the peak emission, in steps of 3%. The peak of the millimeter continuum emission is  $0.67 \text{ Jy beam}^{-1}$ . The synthesized beam of the ALMA continuum image is shown in the lower left corner, in the right image. The color-scale bar on the right panel indicates the peak flux in  $\text{mJy beam}^{-1}$ . The P.A. of the radio thermal jet close to the source is estimated to be around  $137^\circ$ , and the antisymmetric lines shows the jet trajectory associated with a precessing source model (Rodríguez et al. 2008). The r.m.s. noise for the ALMA continuum image is  $7 \text{ mJy beam}^{-1}$ .

southeast direction (position angle: P.A.  $\sim 140^\circ$ ), with the outer lobes symmetrically separated from the central source by an angular distance of  $\sim 10''$ , equivalent to a physical separation in the plane of the sky of  $\sim 0.14 \text{ pc}$  (Garay et al. 2003). The fit to the radio jet by Rodríguez et al. (2008) gives a position angle of  $137^\circ$  within a few arc seconds from the star. It should be noted, however, that at smaller scales the core of the jet shows a somewhat different position angle of  $164^\circ$  (Rodríguez et al. 2008). In this paper, we will adopt as the representative position angle of the jet the value of  $137^\circ$ .

The central source –related to the infrared source IRAS 16547– has a positive spectral index which is consistent with that expected for a radio thermal (free-free) jet, while the spectral index of the lobes suggests a mix of thermal and non-thermal emission (Araudo et al. 2007). The APEX molecular observations of Garay et al. (2007) revealed the presence of a massive and energetic bipolar outflow (flow mass  $\sim 110 M_\odot$ ; mass outflow rate  $\sim 10^{-2} M_\odot \text{ yr}^{-1}$ ; momentum  $\sim 10^3 M_\odot \text{ km s}^{-1}$  and kinetic energy  $10^{48} \text{ erg}$ ) with lobes  $\sim 0.7 \text{ pc}$  in extent and aligned with the thermal jet located at the center of the core.

Very Large Array (VLA) and Submillimeter Array (SMA)

observations with high spatial resolution have revealed a rotating structure associated with IRAS 16547, traced at small scales ( $\sim 50 \text{ AU}$ ) by the  $\text{H}_2\text{O}$  masers and at moderate scales ( $\sim 1000 \text{ AU}$ ) by the thermal emission of  $\text{SO}_2$ . However, both rotating structures have slightly different position angles and most likely are tracing different parts of IRAS 16547. The  $\text{SO}_2$  rotating structure has an east-west orientation (P.A.  $\sim 90^\circ$ ), while the  $\text{H}_2\text{O}$  structure a P.A.  $\sim 40^\circ$ . The poorly resolved structure of the  $\text{SO}_2$  can be modelled as a rotating ring or two separate objects, while the  $\text{H}_2\text{O}$  rotating structure, on the other hand, was suggested to be a compact Keplerian disk surrounding IRAS 16547 (Franco-Hernández et al. 2009).

In this study, we present submillimeter line and continuum observations, made with the Atacama Large Millimeter/Submillimeter Array (ALMA) of the massive protostar IRAS 16547. We report on the detection of a candidate to compact and hot molecular rotating disk with a size of about  $1000 \text{ AU}$  and with an orientation perpendicular to the radio jet emerging from this object. In §2 and 3 we discuss the observations, and results. In §4 we present the discussion and conclusions.

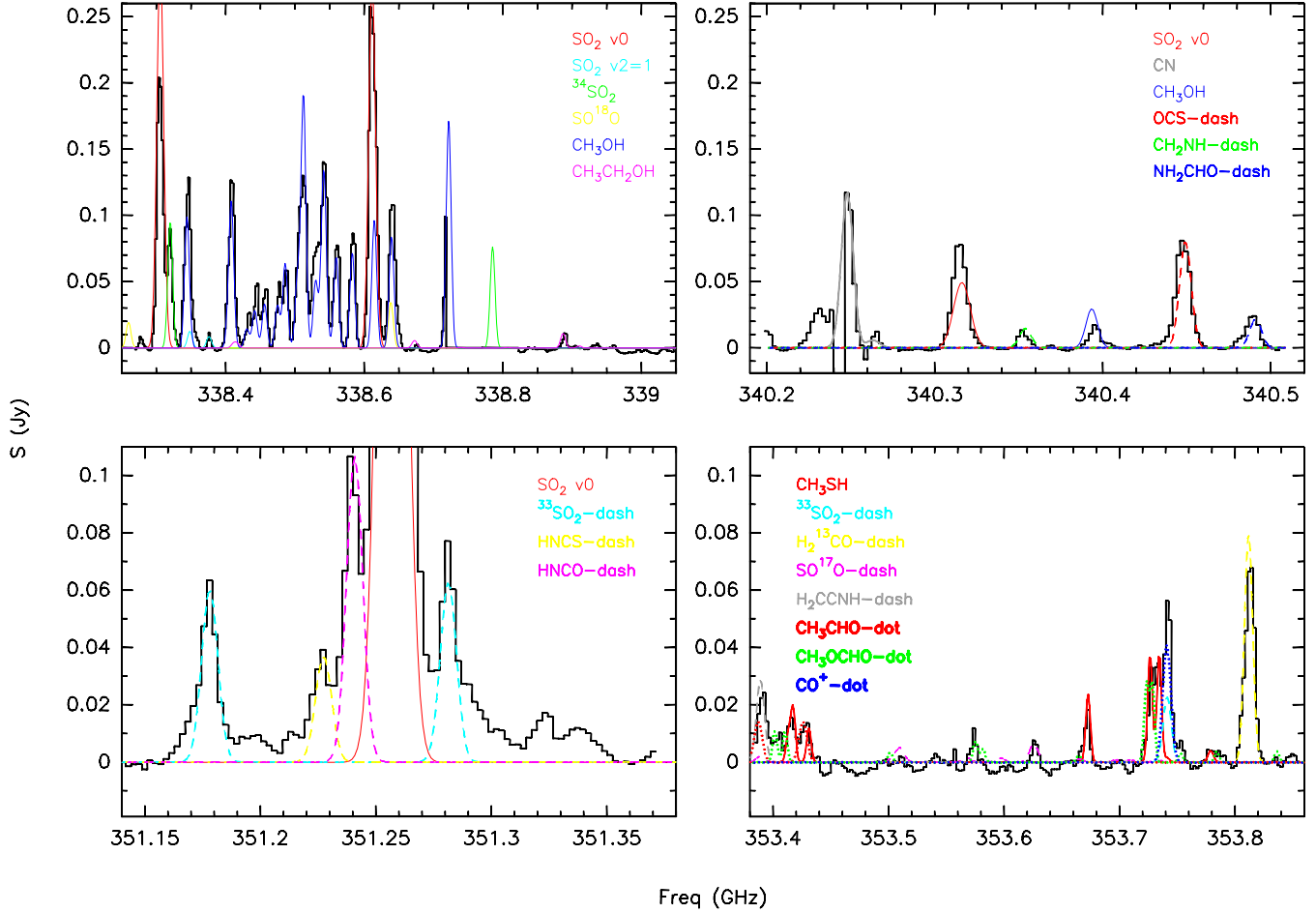


**Figure 2.** Average ALMA spectra obtained from IRAS 16547. The color lines represent the synthetic LTE spectra assuming the parameters described in the text. We remark that this synthetic spectra is only used for line identification.

## 2 OBSERVATIONS

The observations were carried out with 32 antennas of The Atacama Large Millimeter/Submillimeter Array (ALMA) on April (16 antennas) and August 2012 (21 antennas), during the cycle 0 science data program. The array at that point only included antennas with diameters of 12 meters. The 496 independent baselines ranged in projected length from 25 to 364 m.

The phase reference center for the observations was at  $\alpha_{J2000.0} = 16^{\text{h}}58^{\text{m}}17^{\text{s}}.24$ ,  $\delta_{J2000.0} = -42^{\circ}52'08''.09$ , the position of the object IRAS 16547. The primary beam of ALMA at 345 GHz has a FWHM  $\sim 17.6''$ . The dusty emission from IRAS 16547 falls well inside of the FWHM. The ALMA digital correlator was configured in 4 spectral windows of 1875 MHz and 3840 channels each. This provides a spectral resolution of 0.488 MHz ( $\sim 0.4 \text{ km s}^{-1}$ ) per channel. The spectral windows were centered at 350.355 GHz, 352.228 GHz, 340.117 GHz, and 341.971 GHz, in order to detect different spectral lines as for example, SO,  $^{34}\text{SO}$ , and CS. These lines had already been reported toward this massive young stellar object using the single dish telescopes *SEST* and *APEX* (Garay et al. 2003, 2007).

Observations of Titan provided the absolute scale for the flux density calibration. For the time-dependent gain calibration, the nearby quasar J0607–085 was observed approximately every 15 minutes. The quasar 3C279 was used for the bandpass calibration.

The data were calibrated, imaged, and analyzed using the Common Astronomy Software Applications (CASA; McMullin et al. 2007). To analyze the data, we also used the KARMA (Gooch 1996) and AIPS of the National Radio Astronomy Observatory (NRAO) software. In order to construct the continuum image, we used the total bandwidth of the observations (7.5 GHz) selecting only the line-free channels. However, as there are many lines detected in the spectral windows, we have probably some contamination from very faint lines. We used uniform weighting in the continuum and lines maps presented in this study. The resulting r.m.s. noise for the continuum image was  $7 \text{ mJy beam}^{-1}$  at an angular resolution of  $0''.39 \times 0''.34$  with a P.A. =  $69.2^{\circ}$ . For the line emission, the resulting r.m.s. noise was about  $35 \text{ mJy beam}^{-1} \text{ km s}^{-1}$  at the same angular resolution.

## 3 RESULTS

### 3.1 0.85 mm continuum emission

In Figure 1, we present the main results of the ALMA 0.85 mm continuum observations of IRAS 16547. The submillimeter source reported by Garay et al. (2003) was found to have a western extension by Franco-Hernández et al. (2009). We resolved the source into two continuum sources with a clumpy morphology, one of

**Table 1.** Transitions detected toward IRAS 16547

Molecule	Transition	Rest Freq. (GHz)	$S_{ij}^1 \mu^2$ (D <sup>2</sup> )	$E_u$ (K)
SO <sub>2</sub> v=0	18 <sub>4,14</sub> –18 <sub>3,15</sub>	338.30599	26.81	197
	20 <sub>1,19</sub> –19 <sub>2,18</sub>	338.61181	26.02	199
	28 <sub>2,26</sub> –28 <sub>1,27</sub>	340.31641	32.05	392
	5 <sub>3,3</sub> –4 <sub>2,2</sub>	351.25722	7.32	36
SO <sub>2</sub> v <sub>2</sub> =1	4 <sub>3,1</sub> –3 <sub>2,2</sub>	338.34874	7.07	792
	8 <sub>2,6</sub> –7 <sub>1,7</sub>	338.37638	5.09	803
<sup>34</sup> SO <sub>2</sub> v=0	13 <sub>2,12</sub> –12 <sub>1,11</sub>	338.32036	13.59	93
<sup>33</sup> SO <sub>2</sub> v=0	8 <sub>4,4</sub> –8 <sub>3,5</sub> , F=19/2–19/2	351.17796	11.16	73
	9 <sub>4,6</sub> –9 <sub>3,7</sub> , F=21/2–21/2	351.28137	12.88	81
	19 <sub>4,16</sub> –19 <sub>3,17</sub> , F=41/2–41/2	353.74156	25.37	217
SO <sup>18</sup> O	20 <sub>0,20</sub> –19 <sub>1,19</sub>	338.63882	43.41	184
OCS	28–27	340.44927	14.32	237
HNCS <i>a</i> -type	30 <sub>1,30</sub> –29 <sub>1,29</sub>	351.22743	80.60	324
SO <sup>17</sup> O	20 <sub>1,20</sub> –19 <sub>0,19</sub>	353.62533	263.56	186
CH <sub>3</sub> SH	14 <sub>13</sub> –13 <sub>13</sub> –/+A	353.41736	3.32	864
	14 <sub>13</sub> –13 <sub>13</sub> E	353.43107	3.33	863
	14 <sub>9</sub> –13 <sub>9</sub> –/+A	353.67282	14.10	479
	14 <sub>2</sub> –13 <sub>2</sub> –A	353.72626	23.60	147
	14 <sub>8</sub> –13 <sub>8</sub> –/+A	353.73446	16.20	406
	14 <sub>8</sub> –13 <sub>8</sub> E	353.74153	16.27	408
	14 <sub>7</sub> –13 <sub>7</sub> E	353.77778	18.11	341
	14 <sub>7</sub> –13 <sub>7</sub> E	353.78050	18.11	342
CH <sub>3</sub> OH	7 <sub>–1,7</sub> –6 <sub>–1,6</sub>	338.34463	5.54	71
	7 <sub>0,7</sub> –6 <sub>0,6</sub> + +	338.40868	5.66	65
	7 <sub>–6,1</sub> –6 <sub>–6,0</sub>	338.43093	1.50	254
	7 <sub>6,1</sub> –6 <sub>6,0</sub> + +	338.44234	1.49	259
	7 <sub>–5,2</sub> –6 <sub>–5,1</sub>	338.45650	2.76	189
	7 <sub>5,3</sub> –6 <sub>5,2</sub>	338.47529	2.76	201
	7 <sub>5,3</sub> –6 <sub>5,2</sub> + +	338.48634	2.77	203
	7 <sub>2,6</sub> –6 <sub>2,5</sub> – –	338.51286	5.23	103
	7 <sub>4,3</sub> –6 <sub>4,2</sub>	338.53025	3.82	161
	7 <sub>3,5</sub> –6 <sub>3,4</sub> + +	338.54080	4.60	115
	7 <sub>–3,5</sub> –6 <sub>–3,4</sub>	338.55993	4.64	128
	7 <sub>3,4</sub> –6 <sub>3,3</sub>	338.58319	4.62	113
	7 <sub>1,6</sub> –6 <sub>1,5</sub>	338.61500	5.68	86
	7 <sub>2,5</sub> –6 <sub>2,4</sub> + +	338.63994	5.23	103
	7 <sub>2,5</sub> –6 <sub>2,4</sub>	338.72163	5.14	87
	7 <sub>–2,6</sub> –6 <sub>–2,5</sub>	338.72294	5.20	91
	16 <sub>6,10</sub> –17 <sub>5,13</sub> + +	340.39367	3.57	509
CH <sub>3</sub> CH <sub>2</sub> OH	15 <sub>7,8</sub> –15 <sub>6,9</sub>	338.88621	13.67	162
CN v=0	N=3–2, J=7/2–5/2, F=9/2–7/2	340.24777	9.01	33
	N=3–2, J=7/2–5/2, F=5/2–3/2	340.26177	0.59	33
	N=3–2, J=7/2–5/2, F=7/2–5/2	340.26495	0.58	33
CH <sub>2</sub> NH	3 <sub>1,3</sub> –2 <sub>0,2</sub> , F=4–3	340.35431	6.07	26
NH <sub>2</sub> CHO	16 <sub>3,14</sub> –15 <sub>3,13</sub>	340.49109	605.53	166
HNCO v=0	16 <sub>4,13</sub> –15 <sub>4,12</sub>	351.24085	30.93	794
H <sub>2</sub> <sup>13</sup> CO	5 <sub>0,5</sub> –4 <sub>0,4</sub>	353.81187	27.17	51
H <sub>2</sub> CCNH	11 <sub>2,10</sub> –12 <sub>1,12</sub>	353.38912	4.25	97
CH <sub>3</sub> CHO <sup>b</sup>	19 <sub>0,19</sub> –18 <sub>0,18</sub> E	353.38728	239.52	172
	19 <sub>0,19</sub> –18 <sub>0,18</sub> A	353.42595	239.30	172
CH <sub>3</sub> OCHO v=0 <sup>2</sup>	29 <sub>4,25</sub> –28 <sub>4,24</sub> E	353.40185	74.20	274
CH <sub>3</sub> OCHO v=0 <sup>2</sup>	29 <sub>4,25</sub> –28 <sub>4,24</sub> A	353.41059	74.21	274
CH <sub>3</sub> OCHO v=1 <sup>2</sup>	28 <sub>7,21</sub> –27 <sub>7,20</sub> A	353.57558	69.94	461
CH <sub>3</sub> OCHO v=0 <sup>2</sup>	32 <sub>2,31</sub> –31 <sub>2,30</sub> E	353.72360	84.18	290
CH <sub>3</sub> OCHO v=0 <sup>2</sup>	32 <sub>2,31</sub> –31 <sub>2,30</sub> A	353.72862	84.15	290
CO <sup>+</sup>	J=3–2, F=5/2–3/2	353.74126	2.40	34

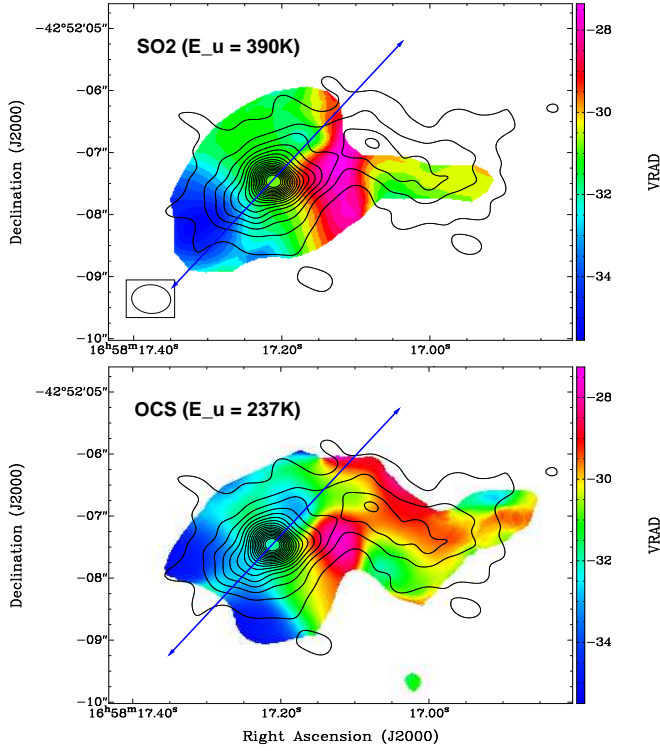


**Figure 3.**  $\text{SO}_2$   $v=0$   $28_{2,26} - 28_{1,27}$ , and  $\text{OCS}$  ( $28-27$ ) thermal emission integrated-intensity weighted velocity (moment one) color maps overlaid with the 0.85 mm continuum maps from IRAS 16547. The black contours show the continuum emission arising at 0.85 mm. The contours range from 5% to 90% of the peak emission, in steps of 5%. The peak of the millimeter continuum emission is  $0.67 \text{ Jy beam}^{-1}$ . The synthesized beam of the ALMA continuum image is shown in the lower left corner of the upper panel. The color-scale bar on the right indicates the LSR radial velocities in  $\text{km s}^{-1}$ . The LSR systemic velocity of IRAS 16547 is  $-30.6 \text{ km s}^{-1}$  (Garay et al. 2003). The blue line in both panels marks the orientation of the thermal (free-free) jet (Rodríguez et al. 2008; Garay et al. 2003) with a P.A. estimated to be around  $137^\circ$ .

them associated with the infrared source IRAS 16547, and the other one  $2''$  to its west (IRAS 16547-W). IRAS 16547-W was already reported by Franco-Hernández et al. (2009) and we find that its peak lies  $\sim 0.4''$  to the west of the centimeter source IRAS 16547 D (Rodríguez et al. 2008).

The continuum source associated with IRAS 16547 is at a position of  $\alpha_{J2000.0} = 16^{\text{h}}58^{\text{m}}17^{\text{s}}211$ ,  $\delta_{J2000.0} = -42^\circ52'07''.47$ . For IRAS 16547-W, it is difficult to obtain a position because of its extended clumpy morphology. The central position of IRAS 16547-W is  $\alpha_{J2000.0} = 16^{\text{h}}58^{\text{m}}17^{\text{s}}051$ ,  $\delta_{J2000.0} = -42^\circ52'07''.11$ . Using a gaussian fitting we found for IRAS 16547 a flux density and peak intensity values of  $2.1 \pm 0.10 \text{ Jy}$  and  $675 \pm 30 \text{ mJy beam}^{-1}$ , respectively. The gaussian fitting was only made in the most central part of IRAS 16547, we do not include the SE-NW extended emission.

For IRAS 16547-W, we found a flux density and peak intensity values of  $1.6 \pm 0.20 \text{ Jy}$  and  $140 \pm 30 \text{ mJy beam}^{-1}$ , respectively. We also find from these fits that the IRAS 16547 source has a de-convolved size of  $0''.56 \pm 0''.02 \times 0''.50 \pm 0''.02$  with a P.A. =  $+115^\circ \pm 5^\circ$ . Therefore, at the distance of this object (2.9 kpc), the size of the continuum source is about  $1620 \text{ AU} \times 1450 \text{ AU}$ .

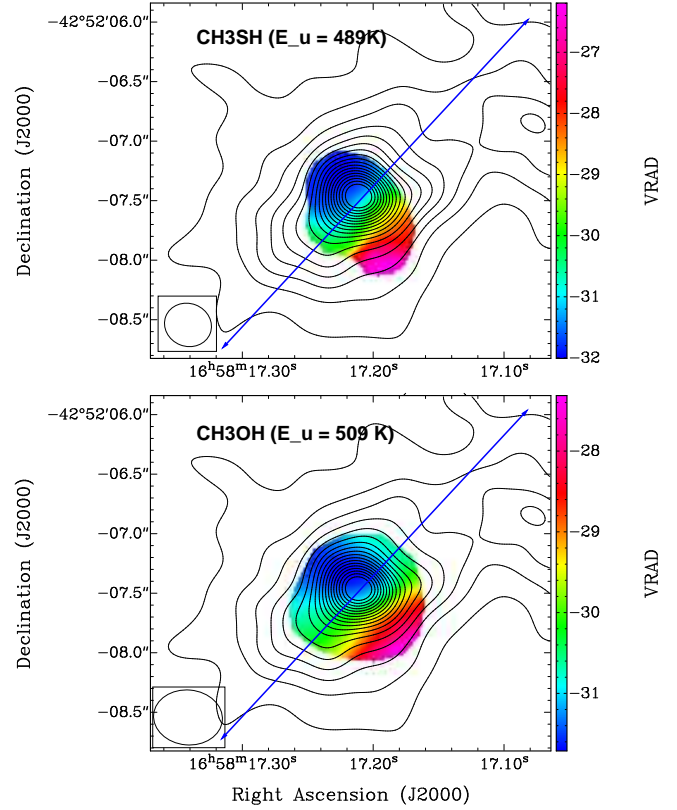


**Figure 4.**  $\text{CH}_3\text{SH}$   $14_9-13_9 -/+A$  and  $\text{CH}_3\text{OH}$   $16_{6,10} - 17_{5,13} ++$  integrated-intensity weighted velocity (first moments) color maps overlaid with the 0.85 mm continuum maps from the innermost parts of IRAS 16547. The black contours show the continuum emission arising at 0.85 mm. The contours range from 5% to 90% of the peak emission, in steps of 5%. The peak of the millimeter continuum emission is  $0.67 \text{ Jy beam}^{-1}$ . The synthesized beam of the ALMA continuum image is shown in the lower left corner. The color-scale bar on the right indicates the LSR radial velocities in  $\text{km s}^{-1}$ . The LSR systemic velocity of IRAS 16547 is  $-30.6 \text{ km s}^{-1}$  (Garay et al. 2003). The blue line in both panels, marks the orientation of the thermal (free-free) jet (Rodríguez et al. 2008; Garay et al. 2003) with a P.A. estimated to be around  $137^\circ$ . The border of the velocity map corresponds to  $3-\sigma$  level.

Assuming that the dust is optically thin and isothermal, and following Hildebrand (1983), the dust mass ( $M_d$ ) will be directly proportional to the flux density ( $S_\nu$ ) as:

$$M = \frac{S_\nu D^2}{B_\nu(T_d) \kappa_\nu}, \quad (1)$$

where  $S_\nu$  is the flux density at the frequency  $\nu$ ,  $D$  is the distance to the Sun,  $B_\nu(T_d)$  is the Planck function at the dust temperature  $T_d$ , and  $\kappa_\nu$  is the absorption coefficient per unit of total (gas+dust) mass density. Writing Eq. (1) in practical units (Palau et al. 2013) :

$$\left[ \frac{M}{M_\odot} \right] = 3.25 \times \frac{e^{0.048 \nu / T_d} - 1}{\nu^3 \kappa_\nu} \times \left[ \frac{S_\nu}{\text{Jy}} \right] \left[ \frac{D}{\text{pc}} \right]^2, \quad (2)$$

where  $T_d$  is in K,  $\nu$  is in GHz, and  $\kappa_\nu$  is in  $\text{cm}^2 \text{g}^{-1}$ . Taking a gas-to-dust ratio of 100, a distance of 2.9 kpc, a dust temperature of 250 K (Hernández-Hernández et al. 2014) for IRAS 16547 and 150 K (this value is uncertain and is obtained more or less from the excitation temperatures of some the lines present in this object) for

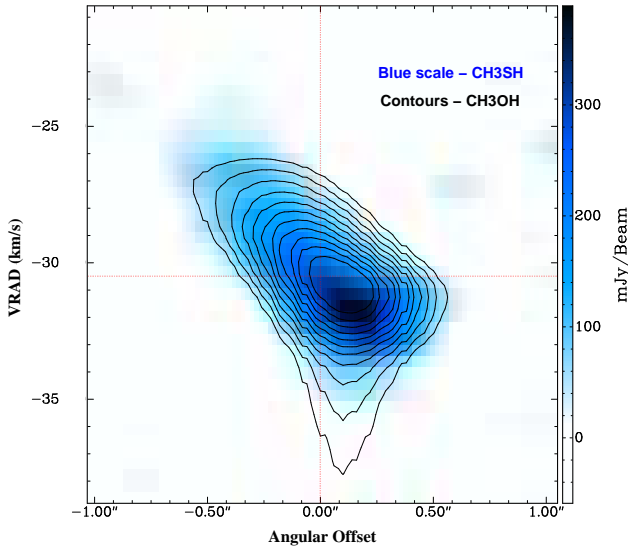


**Figure 5.** Position-velocity diagrams of the  $\text{CH}_3\text{SH}$   $14_9-13_9$   $-/+A$  (blue scale) and  $\text{CH}_3\text{OH}$   $16_{6,10} - 17_{5,13} ++$  (contours) emissions from the innermost parts of IRAS 16547. The contours range from 40% to 90% of the peak emission, in steps of 5%. The peak of the  $\text{CH}_3\text{OH}$  emission is  $1.01 \text{ Jy beam}^{-1}$ . The color-scale bar on the right indicates the peak flux in  $\text{mJy beam}^{-1}$ . The LSR systemic velocity of IRAS 16547 is around  $-30.6 \text{ km s}^{-1}$  (Garay et al. 2003). The spectral and angular resolutions are described in the text. The P.A. for both PV-diagrams ( $\text{CH}_3\text{SH}$  and  $\text{CH}_3\text{OH}$ ) about  $40^\circ$ . The units of the y-axis is in  $\text{km s}^{-1}$ . The angular offset here is relative to the peak of the continuum emission. The positive offsets are measured towards the NE. The  $1-\sigma$  RMS level corresponds to  $35 \text{ mJy beam}^{-1}$ . The radial velocity here is LSR.

IRAS 16547-W, and a dust mass opacity  $\kappa_{850\mu\text{m}} = 0.015 \text{ cm}^2 \text{ g}^{-1}$  (taking into account the gas-to-dust ratio) (Ossenkopf & Henning 1994). We estimate the total mass associated with the dust continuum emission related to the disk in IRAS 16547 of  $6.0 M_\odot$  (integrating in an area  $\sim 1''$ ), and for IRAS 16547-W a mass of  $8.0 M_\odot$ . The values of the masses obtained here for IRAS 16547 and IRAS 16547-W have uncertainties of at least a factor two, due mainly to the error in the determination to the dust mass opacity coefficient at this wavelength.

### 3.2 Line thermal emission

In Table 1 we show all spectral lines detected in these observations. We detected 15 molecular species with different transitions and their isotopologues. In particular, we found a large number of S-bearing molecules, for example the rare molecule methyl mercaptan ( $\text{CH}_3\text{SH}$ ). This molecule has been detected only in two star forming regions (G327 and B1; Gibb et al. 2000; Cernicharo et al. 2012), other than the Galactic Center (Linke et al. 1979) and Orion-KL (Kolesnikov et al. 2014), and is supposed to trace hot regions where desorption from grain mantles is very efficient (Cernicharo et al. 2012).

In order to properly identify the lines detected in the four ALMA spectral windows, we built synthetic spectra for all the possible molecules with transitions within  $\pm 3 \text{ MHz}$  of a given line, and compared the synthetic spectra with the observed spectra in the 4 observed windows, see Figure 2 and Table 1. This allowed us to take into account blending and contributions from transitions of different molecules to a given line. The synthetic spec-

tra were computed assuming Local Thermodynamic Equilibrium and optically thin emission as in Palau et al. (2011), and using the molecular data from the Jet Propulsion Laboratory Pickett et al. (1998) and The Cologne Database for Molecular Spectroscopy Müller et al. (2005). Frequencies and energy levels of methyl mercaptan were taken from the Spectral Line Atlas of Interstellar Molecules (SLAIM, the catalog of Frank Lovas, accessible only through Splatalogue<sup>3</sup>). To build the synthetic spectra, we adopted a linewidth (FWHM) of  $7 \text{ km s}^{-1}$  (except for the  $\text{SO}_2$  lines, for which we used a linewidth of  $10 \text{ km s}^{-1}$ ), and used rotational temperatures in the range  $70\text{--}300 \text{ K}$  (Hernández-Hernández et al. 2014). We then varied the column density until the synthetic spectra reasonably matched the observed spectra.

In Figure 3 we show the first moment or the intensity weighted velocity of the  $\text{SO}_2$   $v=0$   $28_{2,26} - 28_{1,27}$ , and OCS ( $28-27$ ) thermal emission. Emission from these two molecules are present in IRAS 16547 as well as IRAS 16547-W. Both molecules emit at similar systemic LSR velocities. The LSR systemic velocity of IRAS 16547 is  $-30.6 \text{ km s}^{-1}$  (Garay et al. 2003). In both molecules, the thermal emission associated with IRAS 16547 is stronger and more compact than that present in IRAS 16547-W. IRAS 16547 shows a clear velocity gradient of  $7 \text{ km s}^{-1}$  over a distance of  $3''$  (equivalent to  $165 \text{ km s}^{-1} \text{ pc}^{-1}$ ). Franco-Hernández et al. (2009) also reported the detection of the  $\text{SO}_2$  at  $1 \text{ mm}$  in IRAS 16547 with a smaller velocity gradient ( $2 \text{ km s}^{-1}$  over  $3''$  or  $47.6 \text{ km s}^{-1} \text{ pc}^{-1}$ ) at similar scales. This small velocity gradient is probably caused by the lower sensitivity of the Submillimeter Array compared to ALMA. Convolution of the ALMA  $\text{SO}_2$  map to the angular resolution reported in Franco-Hernández et al. (2009) revealed similar results. We also noted that the  $\text{SO}_2$  line mapped in SMA study, has an excitation energy much higher than that observed by Franco-Hernández et al. (2009) ( $118 \text{ K}$ ). The blueshifted gas emission is located to its southeast, while the redshifted gas velocities is at its northwest. In these new ALMA observations, the velocity gradient is seen in both molecules ( $\text{SO}_2$  and OCS), with some redshifted gas associated with IRAS 16547-W.

The first moment or the intensity weighted velocity of the  $\text{CH}_3\text{SH}$   $14_9-13_9$   $-/+A$  and  $\text{CH}_3\text{OH}$   $16_{6,10} - 17_{5,13} ++$  thermal emission is presented in Figure 4. The emission from these two molecules is exclusively present in IRAS 16547, and is resolved with dimensions of  $0''.5 \times 0''.3$  with a P.A.  $= 40^\circ$ , corresponding to  $1450 \text{ AU} \times 870 \text{ AU}$ . There is a clear velocity gradient in both molecules and with an orientation almost perpendicular to that of the thermal jet and the molecules  $\text{SO}_2$  and OCS. The blueshifted gas emission is found to its northeast, while the redshifted is at its southwest.

The kinematics of the gas emission traced by the molecules  $\text{CH}_3\text{SH}$   $14_9-13_9$   $-/+A$  and  $\text{CH}_3\text{OH}$   $16_{6,10} - 17_{5,13} ++$  is presented in the Figure 5. The position angle where this diagram was computed is  $40^\circ$ . This reveals more clearly the velocity gradient observed in Figure 4 with a magnitude of  $8 \text{ km s}^{-1}$  over  $1''$  (equivalent to  $566 \text{ km s}^{-1} \text{ pc}^{-1}$ ). A small contribution of Keplerian velocities is observed to the northeast of the source. The reason why we do not see the full Keplerian motions in this position-velocity diagram is probably because we need to better resolve the innermost parts of the possible disk, where the velocities increment more rapidly. However, there is also the possibility that the motions of the innermost parts of the disk are intrinsically non-Keplerian.

<sup>3</sup> <http://www.splatalogue.net/>



#### 4 DISCUSSION

The ALMA observations towards IRAS 16547 revealed a rich variety of molecular species related to both continuum sources (see Table 1). This molecular emission is present at different scales and temperatures. The molecules presented in Figure 3 (SO<sub>2</sub> or OCS) trace, at scales about 10<sup>4</sup> AU, a clear velocity gradient with a similar orientation to the thermal jet. Some other molecules also detected in this observation (*e.g.* CH<sub>3</sub>OH, CH<sub>2</sub>NH, H<sub>2</sub>CCNH) with similar excitation temperatures in the upper states ( $E_u \sim 300$  K) are tracing similar structures at scales of some 10<sup>4</sup> AU. On the other hand, the maximum velocity that an object with mass  $m$  can achieve under a gravitational field of an object with mass  $M$  can be inferred from a balance between gravity and centrifugal forces:

$$\frac{mv^2}{R} - \frac{GMm}{R^2} = 0,$$

where  $R$  is the distance to the object of mass  $M$  creating the gravitational field,  $G$  is the gravitational constant, and  $v$  is the velocity. This yields a dynamical mass given by

$$M = \frac{Rv^2}{G}.$$

Writing this equation in practical units, we obtain:

$$M[M_\odot] = 1.13 \times 10^{-3} v^2 [km s^{-1}] R[AU].$$

If we assume that the gradient observed in Figure 3 is produced by a rotating structure centered in IRAS 16547, we estimated a dynamical mass of 60  $M_\odot$ . This mass corresponds to an early O-type protostar with a bolometric luminosity of  $\sim 10^6 L_\odot$  (Panagia 1973), which exceeds by one order of magnitude the bolometric luminosity of IRAS 16547 ( $\sim 10^5 L_\odot$ ). We then suggest that this gradient might be produced by the thermal jet that entrains the molecular gas, and that has a similar orientation. Moreover, the emission of the high velocity wings from the SO<sub>2</sub> is very extended in the direction of the jet. We therefore conclude that the SO<sub>2</sub> emission is most likely tracing an outflow.

At much more smaller scales ( $\sim 1000$  AU), molecules with high excitation temperatures ( $E_u \gtrsim 500$  K) trace a compact rotating structure perpendicular to the orientation of the thermal jet (see Figure 4 & 5). This group of molecules includes: SO<sub>2</sub>  $v_2=1$ , HNCO  $v=0$ , CH<sub>3</sub>SH, CH<sub>3</sub>OH, etc. If we do a similar estimation as above, we obtain a dynamical mass of  $\sim 26 M_\odot$ . This value for the mass is uncorrected by the inclination angle. This corresponds to a bolometric luminosity of  $10^{4-5} L_\odot$ , a similar bolometric luminosity to that of IRAS 16547. Given the dimensions, the orientation, and the dynamical mass estimated from the velocity gradient traced by these molecules, we suggest that all these molecules trace an rotating disk surrounding IRAS 16547. Similar results are found for the dynamical mass of the protostar, if we assume that the water masers reported by Franco-Hernández et al. (2009) trace a very compact disk with a similar P.A., and at much more smaller scales ( $\lesssim 300$  AU). An upper limit mass to the disk is  $\sim 6 M_\odot$ , as estimated from the dust thermal emission. In conclusion, removing the mass of the disk, the protostar in the middle has a mass of  $\sim 20 M_\odot$ .

It is interesting to note that even the same molecular species, but in different transitions (*e.g.* SO<sub>2</sub> and SO<sub>2</sub>  $v_2=1$ ) trace distinct components of IRAS 16547. For example, the SO<sub>2</sub>  $v=0$  28<sub>2,26</sub> – 28<sub>1,27</sub> is tracing the outflow (see Figure 3), while the SO<sub>2</sub>  $v_2=1$  8<sub>2,6</sub> – 7<sub>1,7</sub> is tracing the hot disk. This is because of the different excitation temperatures of the molecule at different transitions (see Table 1).

#### 5 CONCLUSIONS

We have carried out submillimeter line and continuum observations made with ALMA of the massive protostar IRAS 16547. The main conclusions of this study are as follows:

- In the 0.85 mm continuum band, the observations revealed two compact sources (with a separation of  $\sim 2''$ ), one of them associated with IRAS 16547–4247, and the other one to the west. Both sources are well resolved angularly, revealing a clumpy structure.
- At scales larger than 10,000 AU, molecules (*e.g.*, SO<sub>2</sub> or OCS) mostly with low excitation temperatures in the upper states ( $E_k \lesssim 300$  K) are present in both millimeter continuum sources, and show a southeast-northwest velocity gradient of  $7 \text{ km s}^{-1}$  over  $3''$  ( $165 \text{ km s}^{-1} \text{ pc}^{-1}$ ). We suggest that this gradient probably is produced by the thermal (free-free) jet emerging from this object with a similar orientation at the base.
- At much smaller scales (about 1000 AU), molecules with high excitation temperatures ( $E_k \gtrsim 500$  K) are tracing a rotating structure elongated perpendicular to the orientation of the thermal jet, which we interpret as a candidate rotating disk surrounding IRAS 16547–4247. From Keplerian arguments, we estimate a mass of about  $20 M_\odot$  for the central star.

#### ACKNOWLEDGEMENTS

L.A.Z., A. P., R. G. and L. F. R. acknowledge the financial support from DGAPA, UNAM, and CONACyT, México. This paper makes use of ALMA data: ADS/JAO.ALMA#2011.0.00419.S. ALMA is a partnership of ESO (representing its member states), NSF (USA), and NINS (Japan), together with NRC (Canada) and NSC and ASIAA (Taiwan), in cooperation with the Republic of Chile. The Joint ALMA Observatory is operated by ESO, AUI/NRAO, and NAOJ.

#### REFERENCES

- Araudo, A. T., Romero, G. E., Bosch-Ramon, V., & Paredes, J. M. 2007, *A&A*, 476, 1289
- Cernicharo, J., Marcelino, N., Roueff, E., et al. 2012, *ApJ*, 759, L43
- Franco-Hernández, R., Moran, J. M., Rodríguez, L. F., & Garay, G. 2009, *ApJ*, 701, 974
- Galván-Madrid, R., Zhang, Q., Keto, E., et al. 2010, *ApJ*, 725, 17
- Garay, G., Brooks, K. J., Mardones, D., & Norris, R. P. 2003, *ApJ*, 587, 739
- Garay, G., Mardones, D., Bronfman, L., et al. 2007, *A&A*, 463, 217
- Gibb, E., Nummelin, A., Irvine, W. M., Whittet, D. C. B., & Bergman, P. 2000, *ApJ*, 545, 309
- Gooch, R. 1996, *Astronomical Data Analysis Software and Systems V*, 101, 80
- Hernández-Hernández, V., Zapata, L., Kurtz, S., & Garay, G. 2014, *ApJ*, 786, 38
- Hildebrand, R. H. 1983, *Quarterly Journal of the Royal Astronomical Society*, 24, 267
- Hoffman, I. M. 2012, *ApJ*, 759, 76
- Jiménez-Serra, I., Zhang, Q., Viti, S., Martín-Pintado, J., & de Wit, W.-J. 2012, *ApJ*, 753, 34
- Klaassen, P. D., Wilson, C. D., Keto, E. R., & Zhang, Q. 2009, *ApJ*, 703, 1308

- Kolesníková, L., Tercero, B., Cernicharo, J., et al. 2014, *ApJ*, 784, L7
- Krumholz, M. R., Klein, R. I., McKee, C. F., Offner, S. S. R., & Cunningham, A. J. 2009, *Science*, 323, 754
- Kuiper, R., Klahr, H., Beuther, H., & Henning, T. 2010, *ApJ*, 722, 1556
- Linke, R. A., Frerking, M. A., & Thaddeus, P. 1979, *ApJ*, 234, L139
- McMullin, J. P., Waters, B., Schiebel, D., Young, W., & Golap, K. 2007, *Astronomical Data Analysis Software and Systems XVI*, 376, 127
- Moscadelli, L., & Goddi, C. 2014, *A&A*, 566, A150
- Müller, H. S. P., Schlöder, F., Stutzki, J., & Winnewisser, G. 2005, *Journal of Molecular Structure*, 742, 215
- Naranjo-Romero, R., Zapata, L. A., Vázquez-Semadeni, E., et al. 2012, *ApJ*, 757, 58
- Ossenkopf, V., & Henning, T. 1994, *A&A*, 291, 943
- Palau, A., Fuente, A., Girart, J. M., et al. 2011, *ApJ*, 743, L32
- Palau, A., Sánchez Contreras, C., Sahai, R., Sánchez-Monge, Á., & Rizzo, J. R. 2013, *MNRAS*, 428, 1537
- Panagia, N. 1973, *AJ*, 78, 929
- Pickett, H. M., Poynter, R. L., Cohen, E. A., et al. 1998, *JQSRT*, 60, 883
- Peters, T., Banerjee, R., Klessen, R. S., et al. 2010, *ApJ*, 711, 1017
- Qiu, K., Zhang, Q., Beuther, H., & Fallscheer, C. 2012, *ApJ*, 756, 170
- Ricci, L., Testi, L., Natta, A., et al. 2010, *A&A*, 512, A15
- Rodríguez, L. F., Moran, J. M., Franco-Hernández, R., et al. 2008, *AJ*, 135, 2370
- Wang, K.-S., van der Tak, F. F. S., & Hogerheijde, M. R. 2012, *A&A*, 543, A22
- Zapata, L. A., Ho, P. T. P., Schilke, P., et al. 2009, *ApJ*, 698, 1422
- Zapata, L. A., Tang, Y.-W., & Leurini, S. 2010, *ApJ*, 725, 1091
- Zapata, L. A., Rodríguez-Garza, C., Rodríguez, L. F., Girart, J. M., & Chen, H.-R. 2011, *ApJ*, 740, L19
- Zinnecker, H., & Yorke, H. W. 2007, *ARAA*, 45, 481